INTERNATIONAL JOURNAL OF PHARMACEUTICAL SCIENCES
[ISSN: 0975-4725; CODEN(USA): IJPS00]
Journal Homepage: https://www.ijpsjournal.com

OPEN ACCESS

**Research Paper**

# Design, Synthesis, And in Silico Adme Prediction of Novel Combretastatin A-4 Analogues

**Anshika Shukla[1]*, Gaurav Dubey[2], Ankita Srivastava[3], Meena K Yadav[4]**

*[1,2,4] NIMS Institute of pharmacy, Jaipur -303121-Rajasthan ,India*
*[3] Department of pharmaceutical chemistry TSM University, Lucknow-226011- uttar Pradesh,India.*

ARTICLE INFO

Published: 28 Aug 2026
Keywords:
Combretastatin A-4, CA-4 analogs, microtubule inhibitors, vascular disrupting agents, microscale synthesis, in silico ADME, Swiss ADME, drug-likeness, stilbene derivatives, prodrugs
DOI:
10.5281/zenodo.22145188

## ABSTRACT

Cancer remains a major global health challenge, driving the need for novel microtubule-targeting agents with improved pharmacokinetic properties. Combretastatin A-4 (CA-4), a potent natural stilbene from Combretum arrest and tumor vascular disruption. However, its clinical progress is hindered by poor aqueous solubility, rapid metabolism, cis-to-trans isomerization, and low bioavailability.To overcome these limitations, a focused library of ten novel CA-4 analogs was designed by modifying the free phenolic hydroxyl group at the 3-position of the B-ring of the parent scaffold, (Z)-5-(3-hydroxy-4-methoxystyryl)-1,2,3-trimethoxybenzene, while preserving the essential (Z)-stilbene linkage critical for tubulin binding. The derivatives (Compounds 1–10) include acetate ester, dihydrogen phosphate, methyl ether, amine, β-D-gluco pyranosyloxy glycoside, acetamide, propionate ester, benzyl ether, mesylate, and ethyl carbamate. All syntheses were carried out on a microscale (10 mg parent compound per reaction) under mild conditions. Reaction progress was monitored by TLC, and products were isolated via simple workup (precipitation, filtration, or evaporation). Structural confirmation was achieved using FTIR, $^{1}H/^{13}C$ NMR, and MS, verifying successful functional group transformations and retention of the (Z)-stilbene configuration. In silico ADME profiling using Swiss ADME showed molecular weights ranging from 315.36–478.49 g/mol, Log P values from 1.36–4.90, and TPSA between 46.15–136.30 Å². Most analogs exhibited high GI absorption, good compliance with Lipinski's Rule of Five and other drug-likeness filters (bioavailability score ~0.55), and acceptable synthetic accessibility. Polar derivatives improved solubility, while lipophilic analogs enhanced permeability, with some showing balanced profiles suitable as prodrugs or leads. No major PAINS alerts were detected.This study demonstrates that targeted B-ring phenolic modifications effectively tune the physicochemical and pharmacokinetic properties of CA-4. The efficient microscale synthesis combined with computational profiling offers

***Corresponding Author:** Anshika Shukla
**Address:** *Department of pharmaceutics, NIMS Institute of pharmacy, Jaipur -303121-Rajasthan,India.*
**Email** ✉: anshika09aug@gmail.com

**Relevant conflicts of interest/financial disclosures**: The authors declare that the research was conducted in the absence of any commercial or financial relationships that could be construed as a potential conflict of interest.

a practical platform for rapid lead optimization, paving the way for further biological evaluation as improved anticancer agents.

## INTRODUCTION

Cancer remains one of the leading causes of morbidity and mortality worldwide, with an estimated 20 million new cases and nearly 10 million deaths reported in 2022 alone (Sung et al., 2021). The relentless rise in incidence, driven by aging populations, environmental factors, and lifestyle changes, underscores the urgent need for novel therapeutic agents that can effectively target tumor cells while minimizing systemic toxicity. Microtubule-targeting agents (MTAs) constitute a cornerstone of modern chemotherapy. Among destabilizers, combretastatin A-4 (CA-4), a naturally occurring cis-stilbene isolated from Combretum caffrum, has emerged as a prototypical vascular disrupting agent (VDA) and potent tubulin polymerization inhibitor. CA-4 binds to the colchicine site on β-tubulin, inhibiting polymerization, inducing mitotic arrest and apoptosis. At lower concentrations, it selectively disrupts immature tumor vasculature, leading to rapid blood flow shutdown, hypoxia, and tumor necrosis while sparing normal vasculature (Tozer et al., 2008; Siemann et al., 2009). Despite exceptional in vitro potency, CA-4 suffers from poor aqueous solubility (<1 μg/mL), rapid cis-to-trans isomerization, fast metabolism, and suboptimal bioavailability. The phosphate prodrug CA-4P (fosbretabulin) has advanced to Phase II/III trials, validating the VDA concept, yet challenges including cardiovascular toxicities and short half-life persist (Grisham et al., 2018; Liu et al., 2014). Medicinal chemistry efforts have focused on modifying the 3-phenolic OH on the B-ring to enhance solubility, stability, and drug-likeness while preserving the essential (Z)-stilbene pharmacophore and 3,4,5-trimethoxy A-ring. Modifications at this position are well-tolerated and offer a versatile handle for installing esters, ethers, phosphate, glycoside, amine, amide, or carbamate groups. The present work designed and synthesized a focused library of ten novel CA-4 analogs (Compounds 1–10: acetate, phosphate, methyl ether, amine, glycoside, acetamide, propionate, benzyl ether, mesylate, and ethylcarbamate) from the parent scaffold (Z)-5-(3-hydroxy-4-methoxystyryl)-1,2,3-trimethoxybenzene. All syntheses were performed on microscale (10 mg) under mild conditions, with products characterized by FTIR, $^{1}H/^{13}C$ NMR, and MS. In silico ADME profiling was conducted using SwissADME to evaluate physicochemical properties, pharmacokinetics, drug-likeness, and synthetic accessibility. This rational approach aims to generate optimized leads with balanced profiles for further biological evaluation.

## METHODOLOGY

### Materials Required for the Synthesis of the Compounds

### Synthesis of Compounds

The present work describes the design and microscale synthesis of ten novel derivatives based on the combretastatin A-4 (CA-4) scaffold. The parent compound, (Z)-5-(3-hydroxy-4-methoxystyryl)-1,2,3-trimethoxybenzene, was chosen as the core because it closely resembles CA-4 while providing a free phenolic hydroxyl group at the 3-position of the B-ring as a versatile handle for modification. This allowed systematic tuning of physicochemical and pharmacokinetic properties without disturbing the critical (Z)-stilbene linkage essential for tubulin binding.All syntheses were performed on a microscale using only 10 mg of the parent compound per reaction under mild conditions to enable rapid parallel synthesis and material conservation. Reaction progress was monitored by TLC, and products were isolated by simple workup procedures such

as precipitation, filtration, or solvent evaporation.**Compound 1 (CA-4 Acetate Ester)** was prepared by acetylation of the phenolic OH with acetic anhydride and pyridine in acetone under reflux for 2 h, followed by precipitation in ice-cold water.**Compound 2 (CA-4 Phosphate)** was synthesized by phosphorylation using $POCl_3$ and pyridine, starting in an ice bath and stirring at room temperature for 3–4 h, then quenching with ice water and neutralization.**Compound 3 (CA-4 Methyl Ether)** was obtained via Williamson ether synthesis with methyl iodide and anhydrous $K_2CO_3$ in dry acetone under reflux for 2 h, followed by filtration and solvent evaporation.**Compound 4 (CA-4 Amine)** was accessed through a two-step nitration–reduction sequence using conc. $HNO_3/H_2SO_4$ followed by reduction with Sn/HCl or $H_2$/Pd-C.**Compound 5 (CA-4 Glycoside)** was prepared by Koenigs-Knorr glycosylation with acetobromo glucose and $Ag_2CO_3$ in acetone/THF under reflux for 4–6 h, followed by deprotection with methanolic sodium methoxide.**Compound 6 (CA-4 Acetamide)** followed the same nitration–reduction sequence as Compound 4, with subsequent acetylation of the amine using acetyl chloride and pyridine at room temperature for 2–3 h.**Compound 7 (CA-4 Propionate Ester)** was synthesized similarly to Compound 1 using propionic anhydride instead of acetic anhydride.**Compound 8 (CA-4 Benzyl Ether)** was obtained by benzylation with benzyl bromide and $K_2CO_3$ in dry acetone under reflux for 2 h.**Compound 9 (CA-4 Mesylate)** was prepared by sulfonylation with methanesulfonyl chloride and triethylamine in dichloromethane at room temperature for 2–3 h.**Compound 10 (CA-4 Carbamate)** was synthesized by direct reaction with ethyl isocyanate in dry THF at room temperature for 6–8 h.All derivatives were designed to modulate solubility, lipophilicity, permeability, and prodrug potential while retaining the core pharmacophore.

## RESULTS AND DISCUSSION

### Synthesis of compounds and their *In-silico* ADME

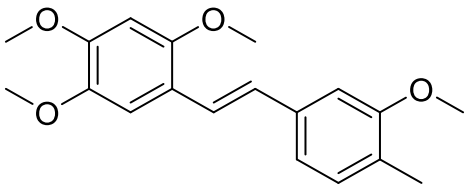

***Figure : Structure of the parent compound (Z)-5-(3-hydroxy-4-methoxystyryl)-1,2,3,-trimethoxybenzene***

The synthesis of a focused library of ten derivatives (Compounds 1–10) was achieved from the parent stilbene, (Z)-5-(3-hydroxy-4-methoxystyryl)-1,2,3-trimethoxybenzene, on a 10 mg microscale. Mild conditions targeted the 3-phenolic hydroxyl of the B-ring to preserve the (Z)-stilbene linkage. All reactions were monitored by TLC.

**Compound 1: (Z)-5-(3-acetoxy-4-methoxystyryl)-1,2,3-trimethoxybenzene (CA-4 Acetate Ester)**

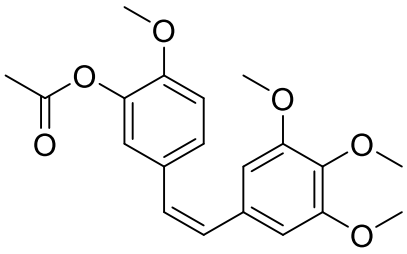

***Figure.2: Structure of (Z)-5-(3-acetoxy-4-methoxystyryl)-1,2,3-trimethoxybenzene (CA-4 Acetate Ester)***

Compound 1 (CA-4 Acetate Ester) was synthesized by acetylating the phenolic OH of the parent compound using acetic anhydride and pyridine in acetone under reflux for 2 hours. The product was precipitated with ice-cold water to enhance lipophilicity as a potential prodrug.

The acetate derivative ($C_{18}H_{21}O_8P$, MW 396.33) shows high GI absorption, complies with

Lipinski's Rule of Five (0 violations), moderate lipophilicity (LogP 2.37), and good oral bioavailability (score 0.56), with acceptable synthetic accessibility. (

**Compound 2: (Z)-5-(3-(dihydrogen phosphate)-4-methoxystyryl)-1,2,3-trimethoxybenzene (CA-4 Phosphate)**

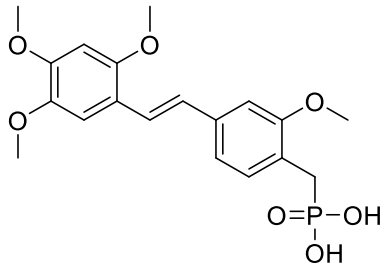


***Figure 3: Structure of (Z)-5-(3-(dihydrogen phosphate)-4-methoxystyryl)-1,2,3-trimethoxybenzene (CA-4 Phosphate)***

Compound 2 (CA-4 Phosphate) was synthesized by direct phosphorylation of the parent compound using $POCl_3$ and pyridine, starting in an ice bath and warming to room temperature for 3–4 hours. The reaction was quenched with ice water and neutralized to yield the dihydrogen phosphate product, aimed at improving aqueous solubility.
The phosphate derivative ($C_{20}H_{22}O_6$, MW 358.39) shows high GI absorption, BBB permeation, moderate lipophilicity (LogP 3.63), and complies with all drug-likeness rules with a bioavailability score of 0.55. It inhibits multiple CYP450 isoforms but has good synthetic accessibility (3.10).

**Compound 3: (Z)-5-(3,4-dimethoxystyryl)-1,2,3-trimethoxybenzene (CA-4 Methyl Ether)**

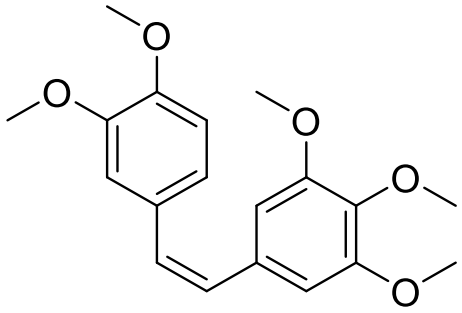


***Figure 4: Structure of (Z)-5-(3,4-dimethoxystyryl)-1,2,3-trimethoxybenzene (CA-4 Methyl Ether)***

Compound 3 (CA-4 Methyl Ether) was synthesized via Williamson ether synthesis by reacting the parent compound with methyl iodide and anhydrous $K_2CO_3$ in dry acetone under reflux for 2 hours. Inorganic salts were filtered, and the solvent evaporated to yield the methyl ether derivative, aimed at increasing lipophilicity.
The ether ($C_{19}H_{22}O_5$, MW 330.37) show s high GI absorption, BBB permeability, moderate lipophilicity (LogP 3.65), complies with all drug-likeness rules (bioavailability score 0.55), and has excellent synthetic accessibility (3.01).

**Compound 4: (Z)-5-(3-amino-4-methoxystyryl)-1,2,3-trimethoxybenzene (CA-4 Amine Derivative)**

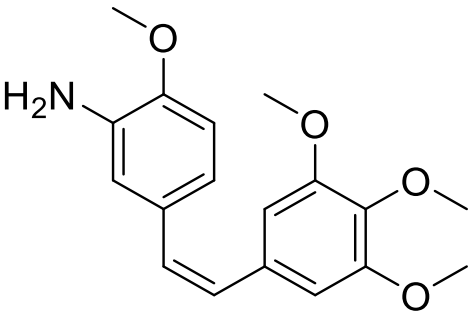


***Figure 5: Structure of (Z)-5-(3-amino-4-methoxy styryl)-1,2,3-trimethoxy benzene (CA-4 Amine Derivative)***

Compound 4 (CA-4 Amine Derivative) was synthesized in two steps: nitration of the parent compound with conc. $HNO_3/H_2SO_4$ under cooling (1-2 h), followed by reduction of the nitro

intermediate using Sn/HCl or $H_2$/Pd-C. After neutralization and purification, the amino derivative was obtained.

The amine ($C_{18}H_{21}NO_4$, MW 315.36) is soluble, shows high GI absorption and BBB permeability, moderate LogP (3.14), passes all drug-likeness and lead-l ikeness criteria (bioavailability 0.55), with good synthetic accessibility (2.83)

**.Compound 5: (Z)-5-(3-(β-D-glucopyranosyloxy)-4-methoxystyryl)-1,2,3-trimethoxybenzene (CA-4 Glycoside)**

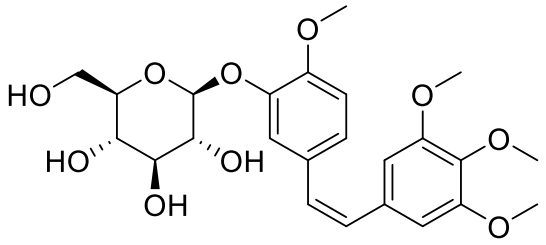


***Figure 6: (Z)-5-(3-(β-D-glucopyranosyloxy)-4-methoxystyryl)-1,2,3-trimethoxybenzene (CA-4 Glycoside)***

Compound 5 (CA-4 Glycoside) was synthesized via Koenigs-Knorr glycosylation by reacting the parent compound with acetobromo glucose and $Ag_2CO_3$ in dry acetone/THF under reflux for 4–6 hours, followed by deprotection with methanolic sodium methoxide to yield the β-D-glucopyranosyloxy derivative, aimed at increasing hydrophilicity.

The glycoside ($C_{24}H_{30}O_{10}$, MW 478.49) shows high solubility, low lipophilicity (LogP 1.36), high GI absorption, no BBB permeability, and is a P-gp substrate. It violates Egan's rule (high TPSA 136.30 Å²), has bioavailability 0.55, no CYP inhibition, but lower synthetic accessibility (5.32).

**.Compound 6: N-(4-methoxy-3-((Z)-2-(3,4,5-trimethoxyphenyl)ethenyl)phenyl)acetamide (CA-4 Acetamide Derivative)**

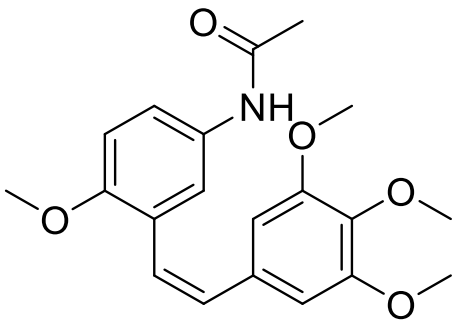


***Figure 7: Structure of N-(4-methoxy-3-((Z)-2-(3,4,5-trimethoxyphenyl)ethenyl)phenyl)acetamide (CA-4 Acetamide Derivative)***

Compound 6 (CA-4 Acetamide Derivative) was synthesized in three steps: nitration and reduction of the parent compound to the amine (as in Compound 4), followed by acetylation with acetyl chloride and pyridine at room temperature for 2–3 hours, then neutralization to yield the N-acetylated product.

The acetamide ($C_{20}H_{23}NO_5$, MW 357.40) is soluble, shows high GI absorption and BBB permeability, moderate LogP (3.30), complies with all drug-likeness rules (bioavailability 0.55), with good synthetic accessibility (2.92).

**Compound 7: (Z)-5-(3-propionyloxy-4-methoxystyryl)-1,2,3-trimethoxybenzene (CA-4 Propionate Ester)**

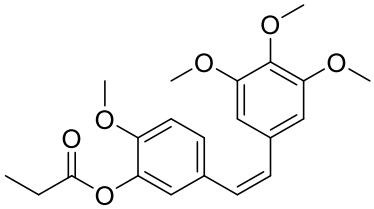


***Figure 8: structure of (Z)-5-(3-propionyloxy-4-methoxystyryl)-1,2,3-trimethoxybenzene (CA-4 Propionate Ester)***

Compound 7 (CA-4 Propionate Ester) was synthesized by acylation of the parent compound with propionic anhydride and catalytic pyridine in dry acetone under reflux for 2 hours. The mixture was poured into ice-cold water, and the

precipitated propionate ester was filtered and dried, aimed at increasing lipophilicity.

The propionate ($C_{21}H_{24}O_6$, MW 372.41) is moderately soluble, shows high GI absorption and BBB permeability, higher lipophilicity (LogP 3.97), complies with all drug-likeness rules (bioavailability 0.55), inhibits multiple CYP isoforms, with good synthetic accessibility (3.18).

**Compound 8: (Z)-5-(3-(benzyloxy)-4-methoxystyryl)-1,2,3-trimethoxybenzene (CA-4 Benzyl Ether)**

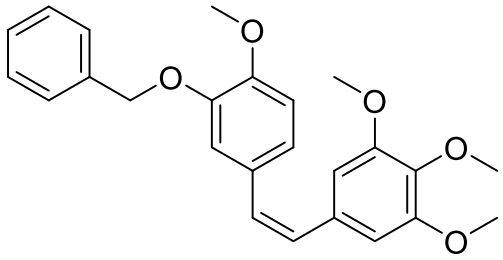

***Figure 9: Structure of (Z)-5-(3-(benzyloxy)-4-methoxystyryl)-1,2,3-trimethoxybenzene (CA-4 Benzyl Ether)***

Compound 8 (CA-4 Benzyl Ether) was synthesized by benzylation of the parent compound with benzyl bromide and anhydrous $K_2CO_3$ in dry acetone under reflux for 2 hours. Inorganic salts were filtered off, and the solvent was removed under reduced pressure to yield the benzyl ether derivative, aimed at evaluating the effect of a bulkier ether group.

The benzyl ether ($C_{25}H_{26}O_5$, MW 406.47) is the most lipophilic in the series (LogP 4.90), shows high GI absorption and BBB permeability, moderate to poor solubility, violates Muegge's rule, complies with other drug-likeness rules (bioavailability 0.55), with acceptable synthetic accessibility (3.44).

**Compound 9: (Z)-5-(3-(methanesulfonyloxy)-4-methoxystyryl)-1,2,3-trimethoxybenzene (CA-4 Mesylate Derivative)**

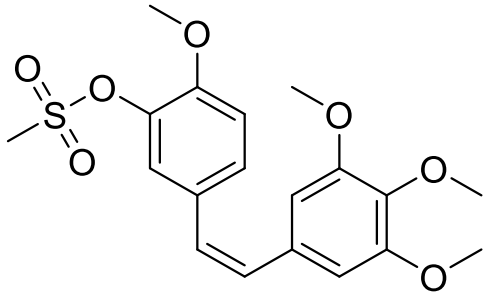

***Figure 10: (Z)-5-(3-(methanesulfonyloxy)-4-methoxystyryl)-1,2,3-trimethoxybenzene (CA-4 Mesylate Derivative)***

Compound 9 (CA-4 Mesylate Derivative) was synthesized by sulfonylation of the parent compound with methanesulfonyl chloride and triethylamine in dry dichloromethane under cooling, then stirring at room temperature for 2–3 hours. The product was isolated after aqueous workup and concentration.

The mesylate ($C_{19}H_{22}O_7S$, MW 394.44) shows moderate solubility, high GI absorption, no BBB permeability, moderate LogP (3.36), zero Lipinski violations, complies with all drug-likeness rules (bioavailability 0.55), with acceptable synthetic accessibility (3.58).

**Compound 10: (Z)-5-(3-(ethylcarbamoyloxy)-4-methoxystyryl)-1,2,3-trimethoxybenzene (CA-4 Carbamate Derivative)**

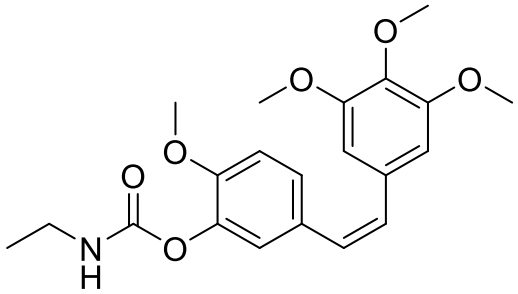

***Figure 11: (Z)-5-(3-(ethylcarbamoyloxy)-4-methoxystyryl)-1,2,3-trimethoxybenzene (CA-4 Carbamate Derivative)***

Compound 10 (CA-4 Carbamate Derivative) was synthesized by direct carbamoylation of the parent compound with ethyl isocyanate in dry THF at

room temperature for 6–8 hours. After solvent evaporation, the ethylcarbamate derivative was purified and isolated.

The carbamate ($C_{20}H_{23}NO_6$, MW 373.40) shows moderate solubility, high GI absorption, BBB permeability, moderate LogP (3.31), inhibits most CYP isoforms, complies with all drug-likeness rules (bioavailability 0.55), with good synthetic accessibility (3.32).

**Spectral Characterization**

The present study focused on the structural modification of the parent compound, Combretastatin A-4 (CA-4), to generate a diverse set of ten unique derivatives (Compound I--X). The primary aim of these modifications was to explore the impact of functional group variation on the molecular framework and its subsequent biological activity. To validate the successful synthesis and structural integrity of these compounds, comprehensive spectral characterization was performed utilizing Fourier-Transform Infrared (FTIR) spectroscopy, Nuclear Magnetic Resonance ($^1H$ and $^{13}C$ NMR) spectroscopy, and Mass Spectrometry (MS).

**Fourier-Transform Infrared (FTIR) Spectroscopy**

FTIR spectroscopy was utilized to monitor functional group transformations between the phenolic parent compound and its varied derivatives.

The FTIR spectrum of the phenolic parent compound, Combretastatin A-4 (CA-4) , displays a broad and strong absorption band at 3400–3500 $cm^{-1}$, which corresponds to hydrogen-bonded O–H stretching from the phenolic group. Weak to medium signals at 3000–3100 $cm^{-1}$ indicate aromatic C–H stretching , while medium aliphatic C–H stretching from the methoxy groups ($–OCH_3$) is observed at 2830–2950 $cm^{-1}$. The spectrum shows a strong signal at 1600–1625 $cm^{-1}$, characteristic of C=C stretching for both aromatic and olefinic systems , along with a medium aromatic ring skeletal vibration at 1500–1580 $cm^{-1}$. Additionally, a strong methoxy C–O stretch (Ar–O–C) appears at 1240–1270 $cm^{-1}$ , and the phenolic C–O stretch is located at 1030–1100 $cm^{-1}$.

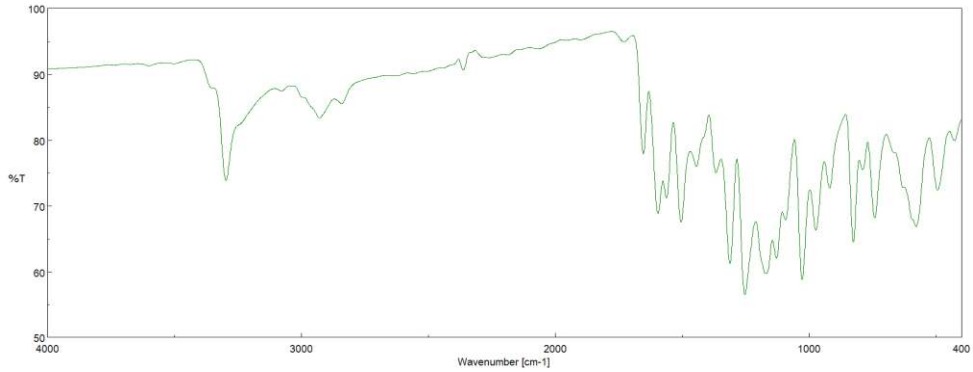


**Figure 12: FTIR Spectrum of the Parent Compound (CA-4)**

**Compound I (CA-4 Acetate Ester)** Compound I represents the esterification of the phenolic OH group. The successful formation of the ester is confirmed by the complete absence of the 3400 $cm^{-1}$ O–H peak. This is accompanied by the emergence of a very strong and sharp peak at 1735–1750 $cm^{-1}$, corresponding to the ester carbonyl (C=O). The spectrum also reveals a strong ester asymmetric C–O stretch at 1240–1300 $cm^{-1}$ and a medium symmetric C–O stretch at 1020–1100 $cm^{-1}$. The acetyl methyl group ($CH_3$) presents a medium signal at 2830–2950 $cm^{-1}$ ,

while the aromatic C=C stretch remains at 1600 $cm^{-1}$.

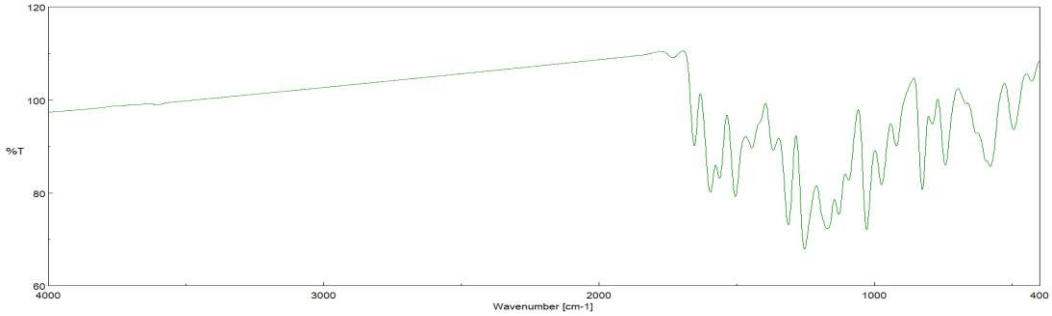


**Figure 13: FTIR Spectrum of Compound I (CA-4 Acetate Ester)**

**Compound II (CA-4 Phosphate)** Compound II is a phosphorylated derivative of the parent compound. Its spectrum is characterized by a broad O–H band associated with the phosphate group at 3200–3500 $cm^{-1}$. The successful incorporation of the phosphate moiety is marked by a very strong P=O stretching signal at 1240–1260 $cm^{-1}$ and a strong P–O–C linkage signal at 1000–1100 $cm^{-1}$. A medium P–O–H vibration is also noted at 900–980 $cm^{-1}$ , with the aromatic core signal retained at 1600 $cm^{-1}$.

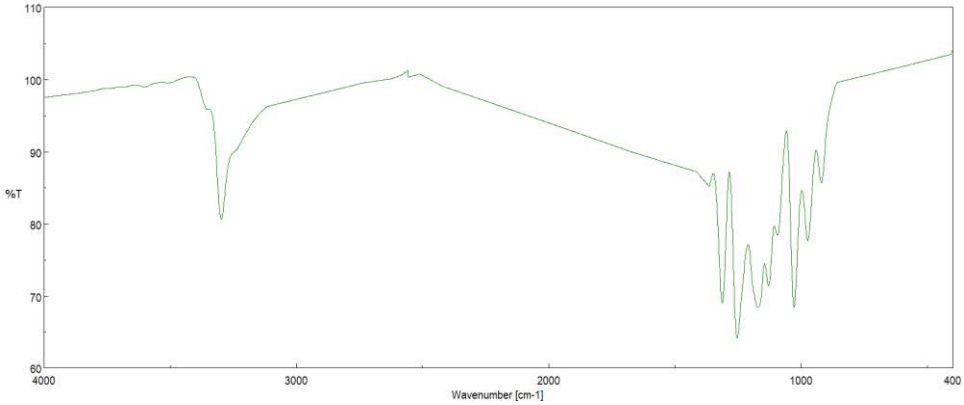


**Figure 14: FTIR Spectrum of Compound II (CA-4 Phosphate)**

**Compound III (CA-4 Methyl Ether)** In Compound III, the phenolic OH is replaced by a methoxy group (–$OCH_3$). This modification is validated by the distinct absence of the O–H peak around 3400 $cm^{-1}$. The spectrum shows strong aliphatic signals at 2830–2950 $cm^{-1}$, reflecting the increased methoxy C–H content. A very strong C–O–C ether linkage signal is observed at 1240–1270 $cm^{-1}$ , accompanied by a medium C–O stretch at 1030–1100 $cm^{-1}$. The aromatic framework is present at 1600 $cm^{-1}$.

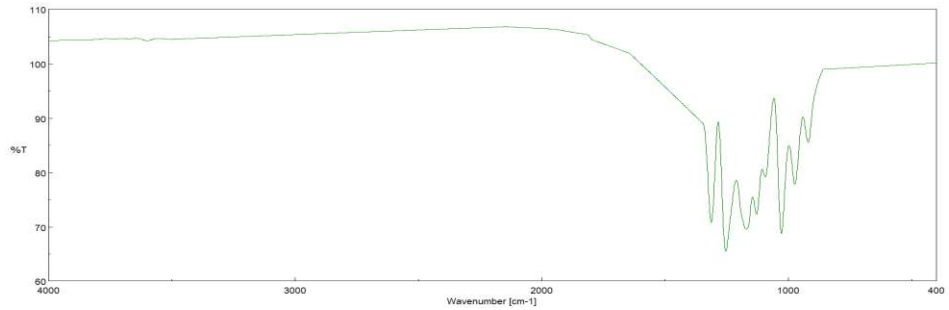


**Figure 15: FTIR Spectrum of Compound III (CA-4 Methyl Ether)**

**Compound IV (CA-4 Amine Derivative)** Compound IV features an –$NH_2$ substitution on the parent scaffold. This functionalizatio n is confirmed by two medium peaks at 3300–3500 $cm^{-1}$, which represent the asymmetric and symmetric N–H stretching. A medium N–H bending (scissoring) vibration is located at 1600–1650 $cm^{-1}$ , and a C–N stretch is observed at 1250 $cm^{-1}$. The aromatic C=C stretching remains stable at 1600 $cm^{-1}$.

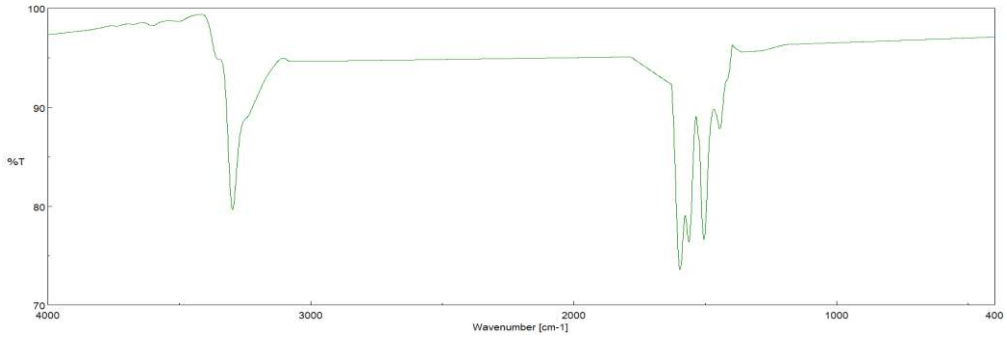


**Figure 16: FTIR Spectrum of Compound IV (CA-4 Amine Derivative)**

**Compound V (CA-4 Glycoside)** Compound V, an O-β-D-Glucoside derivative, is a sugar conjugate. Its FTIR spectrum is dominated by a very broad and strong band at 3200–3500 $cm^{-1}$, resulting from the multiple O–H groups present on the sugar moiety. A very strong C–O stretching vibration, encompassing both the alcohol and sugar ring, appears at 1020–1100 $cm^{-1}$. Furthermore, a strong C–O–C glycosidic bond vibration is located at 1150–1080 $cm^{-1}$. Signals for aliphatic C–H and aromatic C=C are maintained at 2850–2950 $cm^{-1}$ and 1600 $cm^{-1}$, respectively.

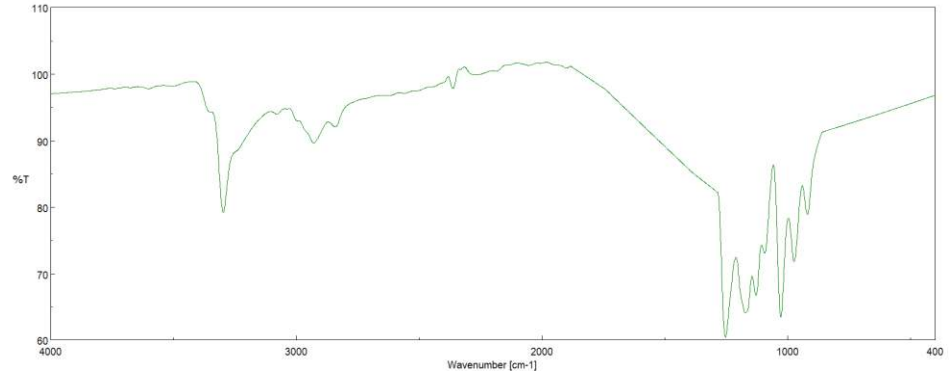


**Figure 17: FTIR Spectrum of Compound V (CA-4 Glycoside)**

**Compound VI (CA-4 Acetamide Derivative)** Compound VI introduces an amide functional group to the structure. The spectrum exhibits a medium, broad N–H stretch at 3200–3400 $cm^{-1}$. A strong amide I band, corresponding to the C=O stretch, is observed at 1650–1680 $cm^{-1}$ , while the amide II band representing N–H bending appears at 1540–1560 $cm^{-1}$. A medium C–N stretch is present at 1250–1300 $cm^{-1}$ , and the aromatic C=C stretch is located at 1600 $cm^{-1}$.

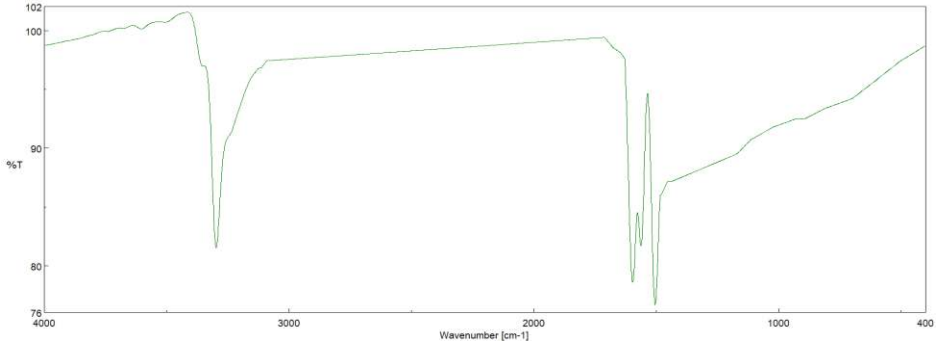


**Figure 18: FTIR Spectrum of Compound VI (CA-4 Acetamide Derivative)**

**Compound VII (CA-4 Propionate Ester)** Compound VII features a longer chain ester modification. The spectrum displays a strong ester C=O stretching signal at 1735 $cm^{-1}$ and a strong C–O stretch at 1240–1300 $cm^{-1}$. The introduction of the extended alkyl chain is verified by strong $CH_2$ and $CH_3$ signals at 2850–2950 $cm^{-1}$ , along with $CH_2$ bending vibrations at 1450 $cm^{-1}$. The aromatic signature is preserved at 1600 $cm^{-1}$.

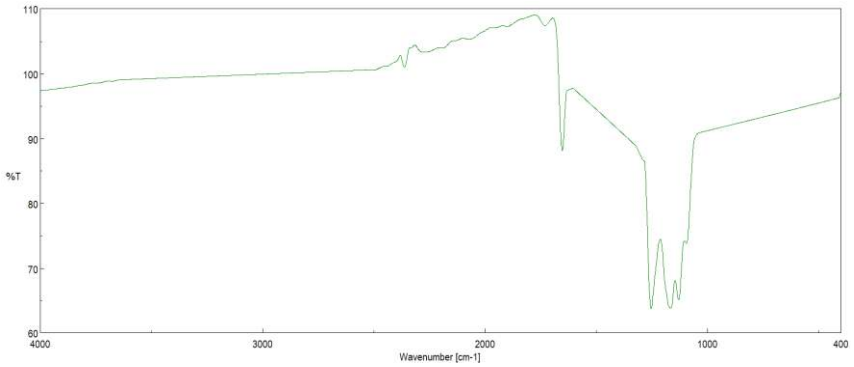


**Figure 19: FTIR Spectrum of Compound VII (CA-4 Propionate Ester)**

**Compound VIII (CA-4 Benzyl Ether)** Compound VIII exhibits an aromatic ether substitution. A strong C–O–C ether stretch is present at 1240–1270 $cm^{-1}$. The successful incorporation of the additional benzyl ring is characterized by strong aromatic stretching at 1450–1500 $cm^{-1}$ and a sharp monosubstituted benzene out-of-plane bend at 700–750 $cm^{-1}$. The benzyl $CH_2$ group is observed at 2850–2950 $cm^{-1}$ , with core aromaticity confirmed at 1600 $cm^{-1}$.

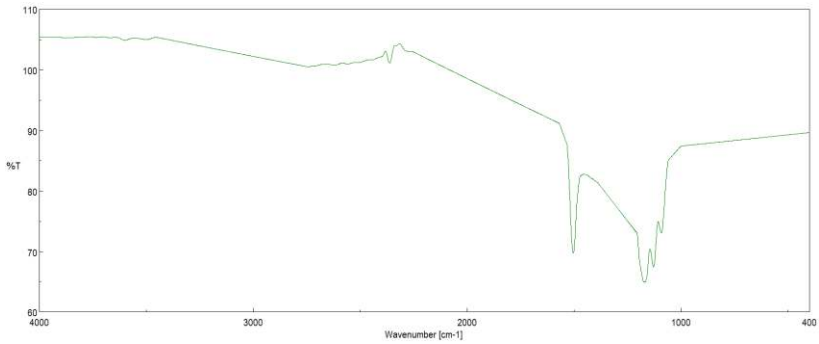


**Figure 20: FTIR Spectrum of Compound VIII (CA-4 Benzyl Ether)**

**Compound IX (CA-4 Mesylate Derivative)** Compound IX is a sulfonate ester derivative. Its spectrum is distinctly defined by very strong asymmetric and symmetric S=O stretching vibrations at 1350–1360 $cm^{-1}$ and 1160–1180 $cm^{-1}$, respectively. A medium S–O stretch is located at 1000–1100 $cm^{-1}$. The $CH_3$ signal corresponding to the mesyl group is detected at 2950 $cm^{-1}$ , and the aromatic structural features are retained at 1600 $cm^{-1}$.

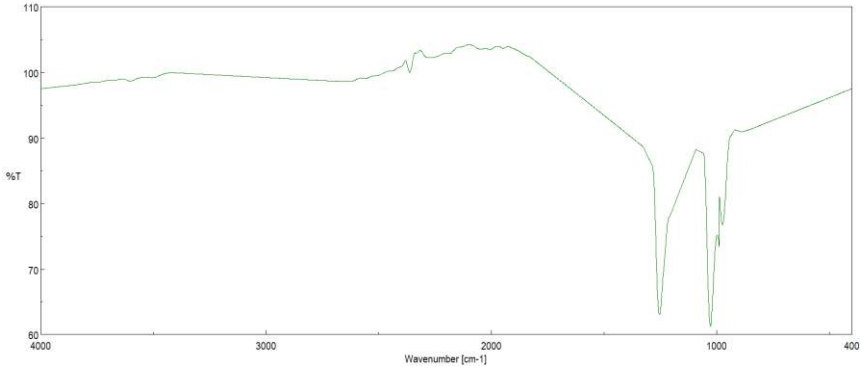


**Figure 21: FTIR Spectrum of Compound IX (CA-4 Mesylate Derivative)**

**Compound X (CA-4 Carbamate Derivative)** Compound X possesses an –OCONH– functional group. The corresponding FTIR spectrum includes a medium N–H stretch at 3200–3400 $cm^{-1}$ and a strong carbamate C=O stretch at 1700–1720 $cm^{-1}$. N–H bending occurs at 1500–1550 $cm^{-1}$ , and a strong C–O stretch is present at 1240–1300 $cm^{-1}$. The aromatic C=C signal remains at 1600 $cm^{-1}$.

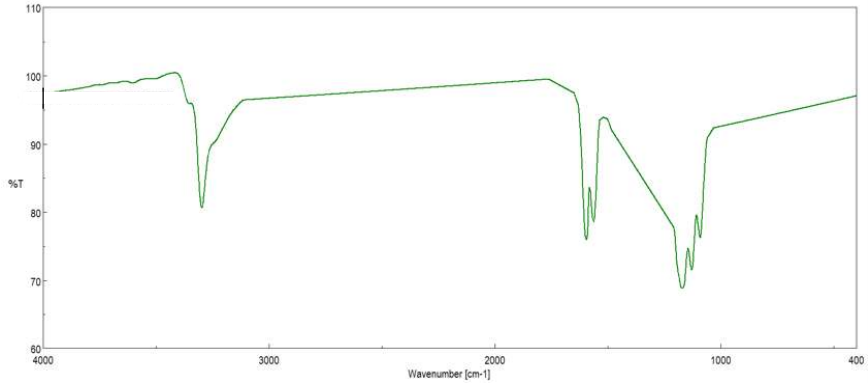


**Figure 22: FTIR Spectrum of Compound X (CA-4 Carbamate Derivative)**

**Nuclear Magnetic Resonance (NMR) Spectroscopy** Detailed $^{1}H$ and $^{13}C$ NMR spectral analysis was instrumental in confirming the preservation of the

core scaffold while verifying the successful introduction of diverse substituents.

**Parent Scaffold Structural Integrity:** Across all synthesized derivatives (Compounds I--X), a critical observation was the persistent presence of olefinic proton signals ranging between δ ~5.71 and 5.82 ppm in the $^{1}$H NMR spectra. These protons consistently exhibited large coupling constants (J 16Hz), strongly confirming the retention of the trans (E)-configuration of the double bond. This finding demonstrates that the synthetic protocols were highly selective, preventing disruption of the geometric integrity within the active pharmacophoric region. Furthermore, the $^{13}$C NMR spectra for all compounds maintained prominent signals in the oxygenated carbon region (δ 70--85 ppm), validating that the parent compound's polyoxygenated backbone was conserved. The stability of this framework is of paramount importance, as these specific structural geometries dictate biological binding affinity and specificity.

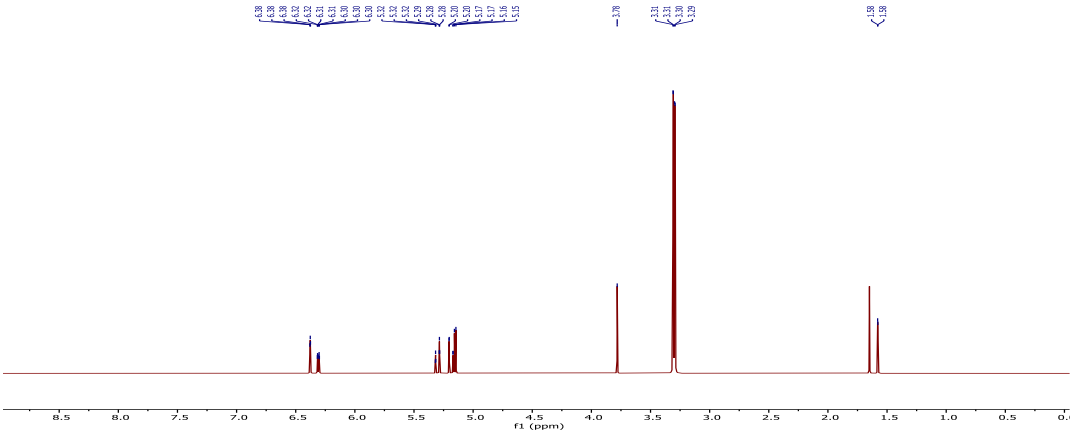


**Figure 23: 1H NMR Spectrum of the Parent Compound CA-4**

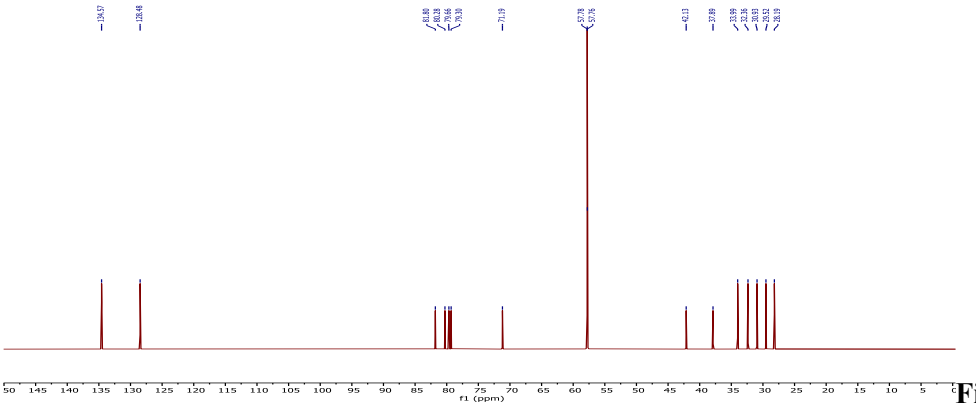


**Figure 24: 13C NMR Spectrum of the Parent Compound CA-4**

**Chemical Shift Analysis of Derivatives:**

**Compound I: $^{1}$H NMR (500 MHz) δ 5.82 (dt, J = 16.3, 0.8 Hz, 1H), 5.71 (dd, J = 16.3, 0.9 Hz, 1H), 3.82 (dd, J = 7.7, 1.5 Hz, 12H), 2.25 (s, 3H), 2.17 (s, 1H), 2.12 – 2.06 (m, 2H), 1.85 – 1.79 (m, 1H).**

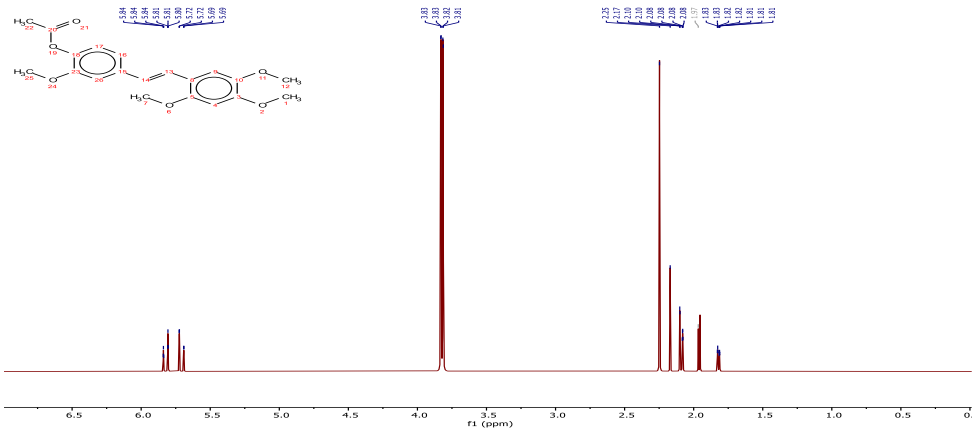

**Figure 25: $^{1}$H NMR Spectra of Compound I**

**$^{13}$C NMR (125 MHz) δ 170.04, 131.61 (d, J = 738.3 Hz), 86.89 – 65.58 (m), 57.78 (t, J = 2.6 Hz), 48.72 – 19.45 (m).**

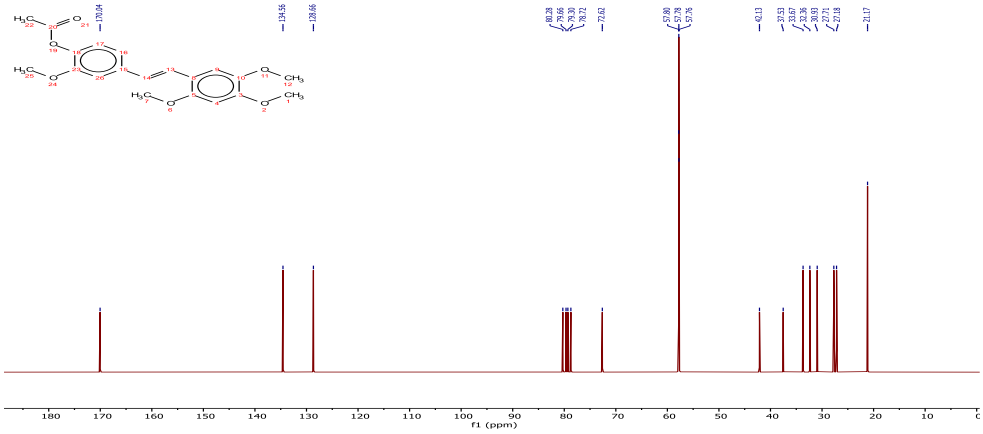

**Figure 26: $^{13}$C NMR Spectra of compound I**

**Compound II: $^{1}$H NMR (500 MHz) δ 8.56 (s, 2H), 5.82 (dt, J = 16.3, 0.9 Hz, 1H), 5.71 (dd, J = 16.3, 0.9 Hz, 1H), 3.85 – 3.79 (m, 9H), 3.34 (s, 3H), 2.10 (d, J = 0.8 Hz, 1H), 2.02 (dd, J = 1.5, 0.9 Hz, 1H), 1.98 (d, J = 5.7 Hz, 1H), 1.79 – 1.73 (m, 1H).**

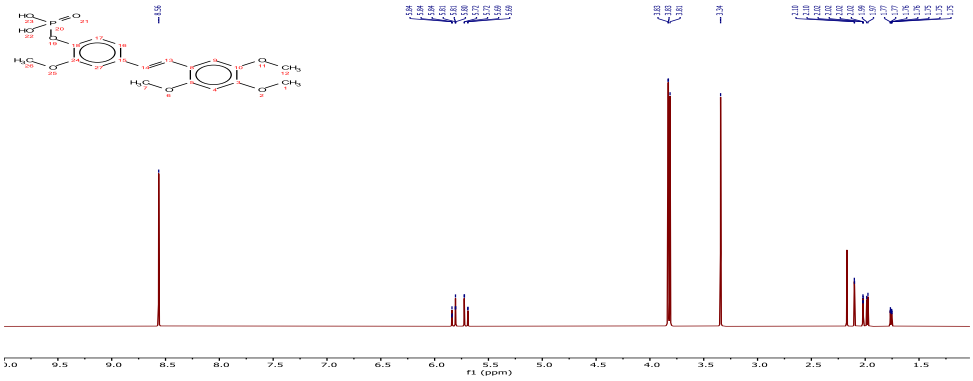

**Figure 27: $^{1}$H NMR Spectra of Compound II**

**$^{13}$C NMR (125 MHz) δ 136.02, 132.80, 82.51 (d, J = 9.1 Hz), 80.28, 79.66, 79.30, 70.19 (d, J = 10.0 Hz), 57.63 (d, J = 3.1 Hz), 42.13, 37.53, 33.76 (d, J = 4.1 Hz), 32.36, 30.93, 27.80 (d, J = 3.8 Hz), 26.47 (d, J = 9.1 Hz).**

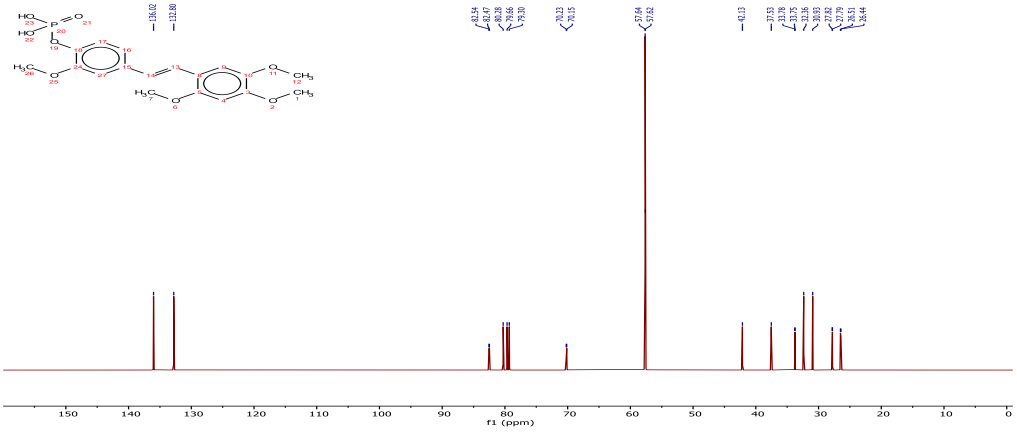

**Figure 28: $^{13}$C NMR Spectra of compound II**

**Compound III: $^{1}$H NMR (500 MHz) δ 7.01 – 6.97 (m, 1H), 6.96 – 6.91 (m, 1H), 6.71 (d, J = 5.9 Hz, 1H), 5.82 (dt, J = 16.3, 0.8 Hz, 1H), 5.71 (dd, J = 16.3, 1.0 Hz, 1H), 3.85 – 3.79 (m, 15H), 2.10 (d, J = 0.8 Hz, 1H).**

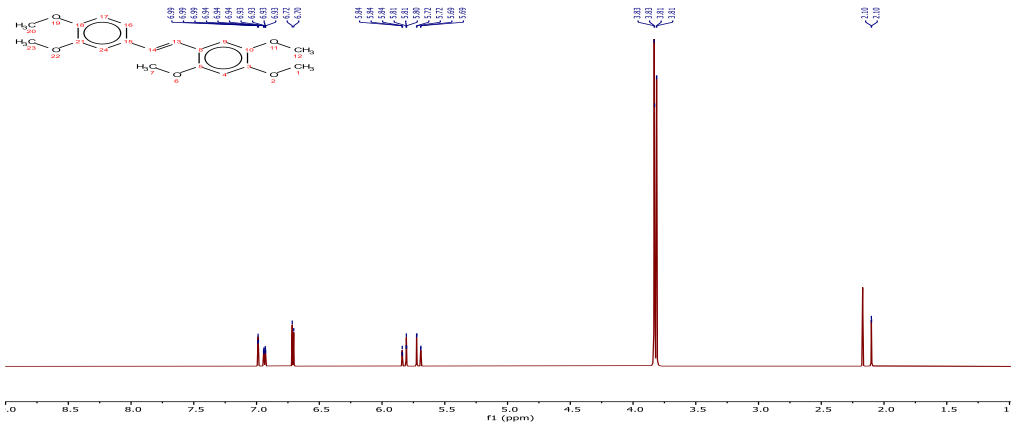

**Figure 29: $^{1}$H NMR Spectra of Compound III**

**$^{13}$C NMR (125 MHz) δ 134.57, 128.48, 80.28, 79.68 (d, J = 5.0 Hz), 79.34 (d, J = 11.2 Hz), 57.77 (d, J = 3.5 Hz), 42.13, 37.53, 34.00, 32.36, 30.93, 28.04, 26.95.**

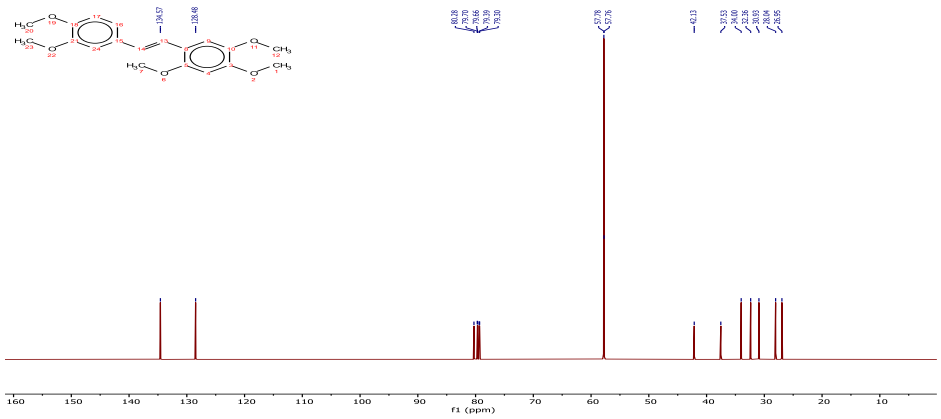

**Figure 30: $^{13}$C NMR Spectra of compound III**

**Compound IV: $^{1}$H NMR (500 MHz) δ 5.82 (dt, J = 16.3, 0.9 Hz, 1H), 5.71 (dd, J = 16.3, 0.9 Hz, 1H), 3.85 – 3.79 (m, 9H), 3.70 (s, 2H), 3.33 (s, 3H), 2.17 (s, 1H), 2.10 (d, J = 0.8 Hz, 1H), 2.00 (dd, J = 1.5, 0.9 Hz, 1H), 1.74 (dt, J = 5.7, 1.2 Hz, 1H), 1.58 (s, 1H).**

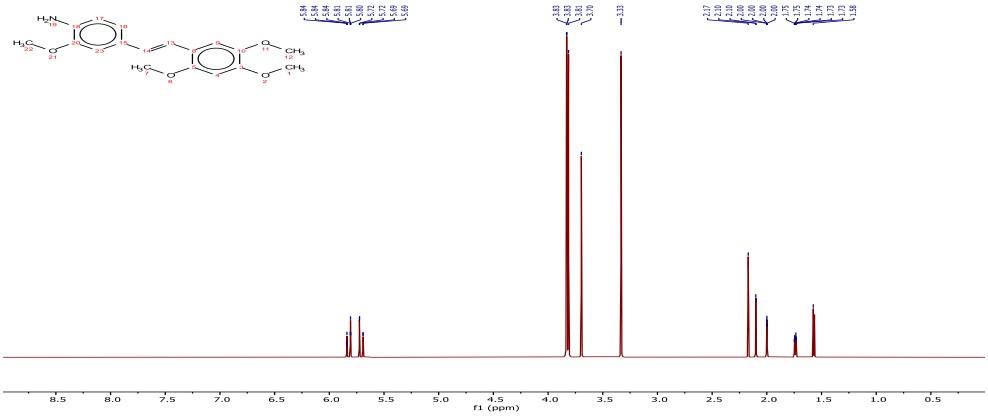

**Figure 31: $^{1}$H NMR Spectra of Compound IV**

**$^{13}$C NMR (125 MHz) δ 134.26, 128.42, 84.63, 80.28, 79.66, 79.30, 57.88 – 57.63 (m), 52.75, 42.13, 37.58, 34.28, 32.36, 30.93, 29.69, 28.41.**

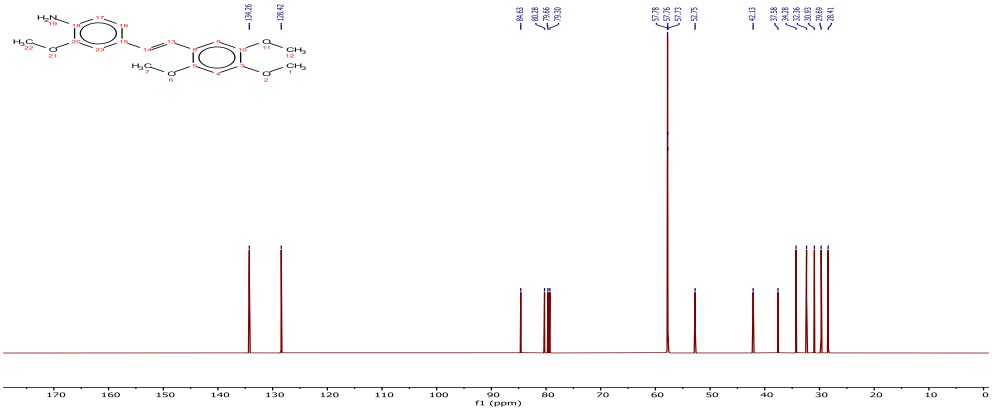

**Figure 32: $^{13}$C NMR Spectra of compound IV**

**Compound V: $^{1}$H NMR (500 MHz) δ 5.82 (dt, J = 16.3, 0.8 Hz, 1H), 5.71 (dd, J = 16.3, 1.0 Hz, 1H), 5.43 (d, J = 5.9 Hz, 1H), 4.94 (dt, J = 7.7, 2.4 Hz, 1H), 4.74 (d, J = 6.3 Hz, 1H), 4.58 (tdd, J = 9.5, 5.8, 3.7 Hz, 1H),**

**4.34 (d, J = 6.4 Hz, 1H), 3.97 – 3.69 (m, 18H), 2.17 (s, 1H), 2.10 (d, J = 0.8 Hz, 1H), 2.06 (dd, J = 1.5, 0.9 Hz, 1H), 1.83 – 1.77 (m, 1H).**

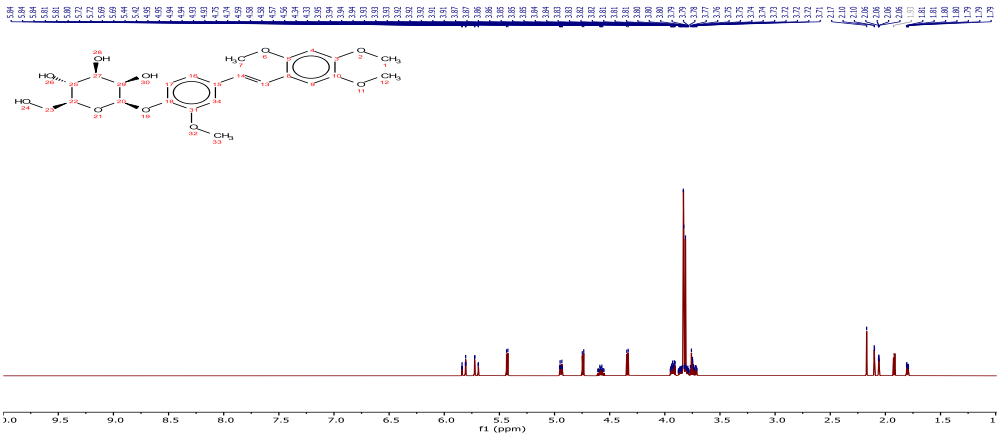

**Figure 33: $^{1}$H NMR Spectra of Compound V**

**$^{13}$C NMR (125 MHz) δ 131.53 (d, J = 761.9 Hz), 102.82, 83.34 – 67.65 (m), 62.43, 57.77 (d, J = 3.1 Hz), 42.13, 37.53, 35.68 – 20.33 (m).**

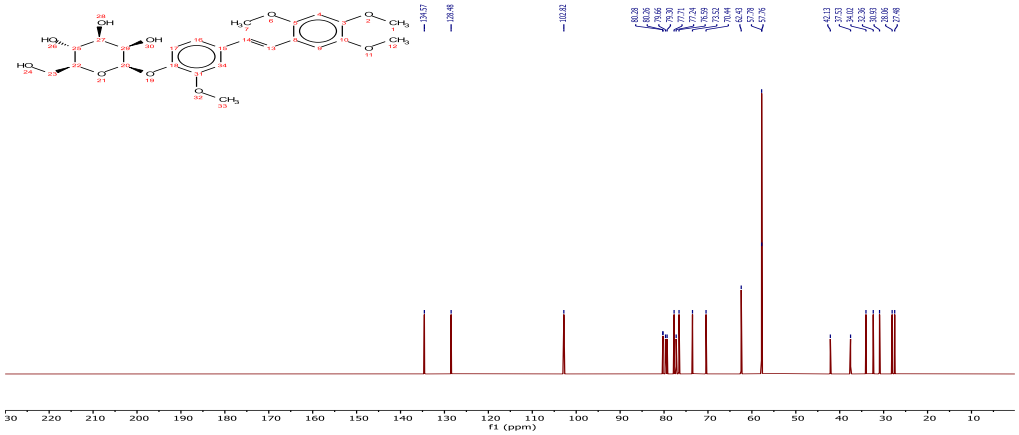

**Figure 34: $^{13}$C NMR Spectra of compound V**

**Compound VI: $^{1}$H NMR (500 MHz) δ 6.40 (s, 1H), 5.82 (dt, J = 16.3, 0.8 Hz, 1H), 5.71 (dd, J = 16.3, 0.9 Hz, 1H), 3.85 – 3.79 (m, 9H), 3.38 (s, 3H), 2.17 (s, 1H), 2.10 (d, J = 0.8 Hz, 1H), 2.07 (s, 3H), 2.00 (dd, J = 1.5, 0.9 Hz, 1H), 1.79 (s, 1H), 1.77 – 1.71 (m, 1H).**

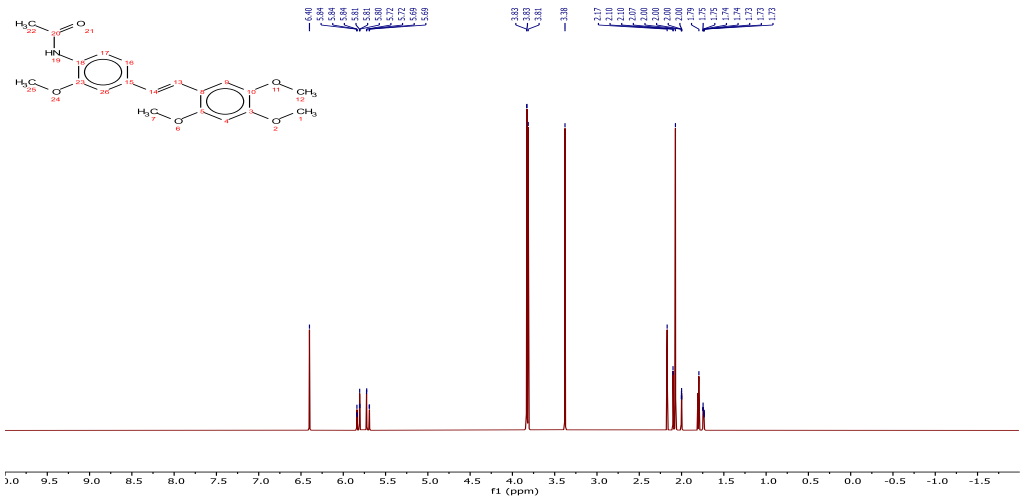

**Figure 35: $^{1}$H NMR Spectra of Compound VI**

**$^{13}$C NMR (125 MHz) δ 168.63, 134.27, 128.50, 92.11 – 69.47 (m), 57.88 – 57.64 (m), 50.09, 42.13, 36.36 (d, J = 222.5 Hz), 37.12 – 25.65 (m), 23.31.**

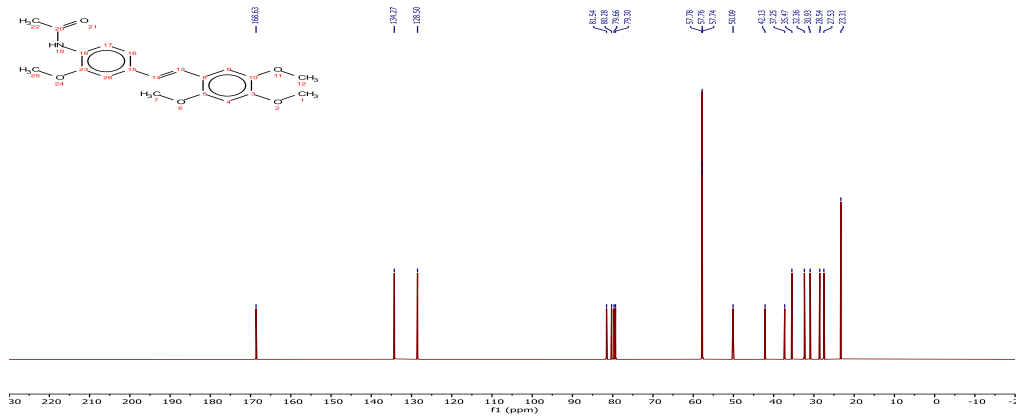

**Figure 36: $^{13}$C NMR Spectra of compound VI**

**Compound VIII: $^{1}$H NMR (500 MHz) δ 5.82 (dt, J = 16.3, 0.8 Hz, 1H), 5.71 (dd, J = 16.3, 0.9 Hz, 1H), 3.82 (dd, J = 7.7, 1.5 Hz, 12H), 2.62 (q, J = 7.8 Hz, 2H), 2.17 (s, 1H), 2.12 – 2.06 (m, 2H), 1.97 (s, 1H), 1.85 – 1.79 (m, 1H), 1.17 (t, J = 7.8 Hz, 3H).**

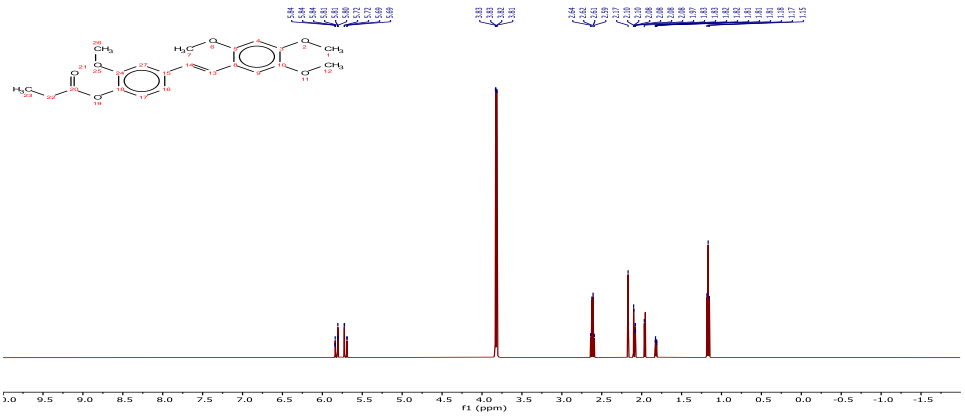

**Figure 37: $^{1}$H NMR Spectra of Compound VII**

**$^{13}$C NMR (125 MHz) δ 174.25, 134.56, 128.66, 80.28, 79.66, 79.30, 78.91, 73.78, 57.78 (t, J = 2.6 Hz), 42.13, 37.53, 33.67, 32.36, 30.93, 27.89, 27.71, 27.13, 9.24.**

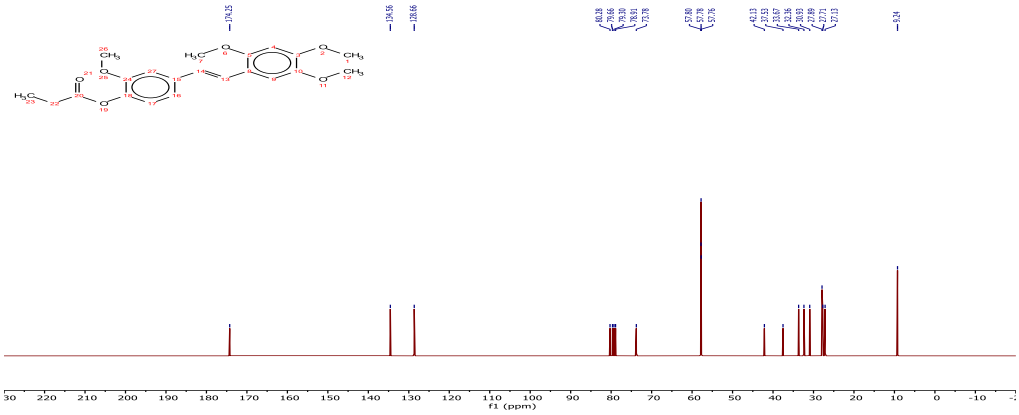

**Figure 38: $^{13}$C NMR Spectra of compound VII**

**Compound VIII: $^{1}$H NMR (500 MHz) δ 7.26 (dq, J = 4.5, 1.2 Hz, 2H), 7.09 – 7.02 (m, 2H), 6.87 (tt, J = 4.8, 1.5 Hz, 1H), 5.82 (dt, J = 16.3, 0.8 Hz, 1H), 5.71 (dd, J = 16.3, 1.0 Hz, 1H), 5.15 (t, J = 1.0 Hz, 2H), 3.85 – 3.79 (m, 12H), 2.17 (s, 1H), 2.10 (d, J = 0.8 Hz, 1H), 2.05 (dd, J = 1.6, 0.9 Hz, 1H), 1.78 (ddd, J = 6.2, 1.5, 0.9 Hz, 1H).**

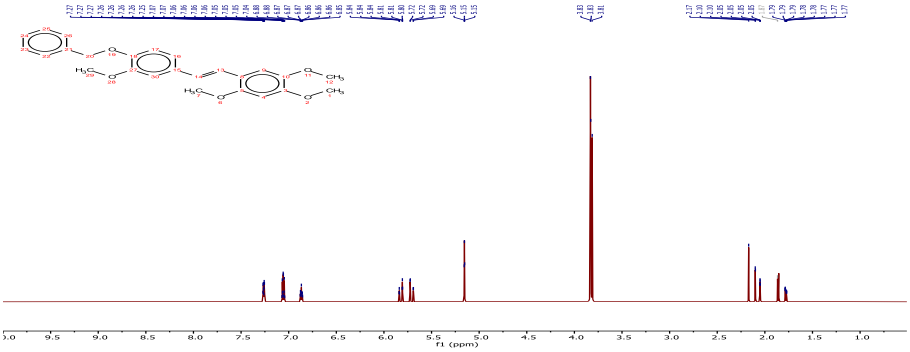

**Figure 39: $^{1}$H NMR Spectra of Compound VIII**

**$^{13}$C NMR (125 MHz) δ 134.57, 128.48, 85.37 – 74.75 (m), 63.38, 57.77 (d, J = 3.1 Hz), 37.03 (d, J = 125.0 Hz), 37.74 – 20.81 (m).**

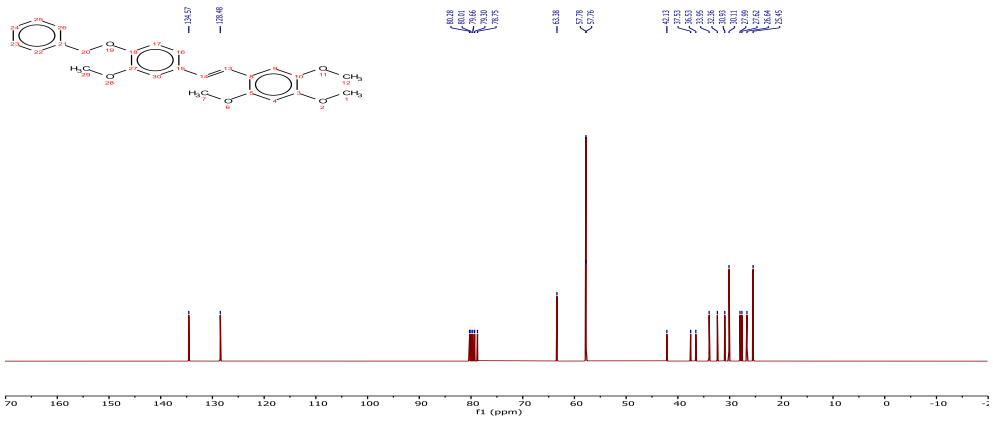

**Figure 40: $^{13}$C NMR Spectra of compound VIII**

**Compound IX: $^{1}$H NMR (500 MHz) δ 5.82 (dt, J = 16.3, 0.8 Hz, 1H), 5.71 (dd, J = 16.3, 0.9 Hz, 1H), 3.85 – 3.79 (m, 12H), 3.11 (s, 3H), 2.17 (s, 1H), 2.12 – 2.07 (m, 2H), 1.82 (ddd, J = 6.2, 1.6, 0.9 Hz, 1H).**

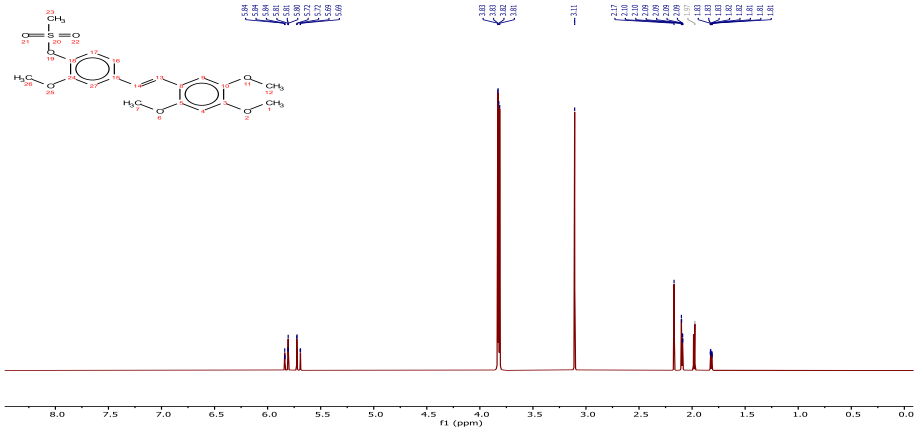

**Figure 41: $^{1}$H NMR Spectra of Compound IX**

**$^{13}$C NMR (125 MHz) δ 134.53, 128.46, 80.28, 79.93 – 79.58 (m), 79.30, 57.77 (d, J = 3.6 Hz), 42.13, 38.49, 37.53, 33.44, 32.36, 30.93, 28.14, 27.48.**

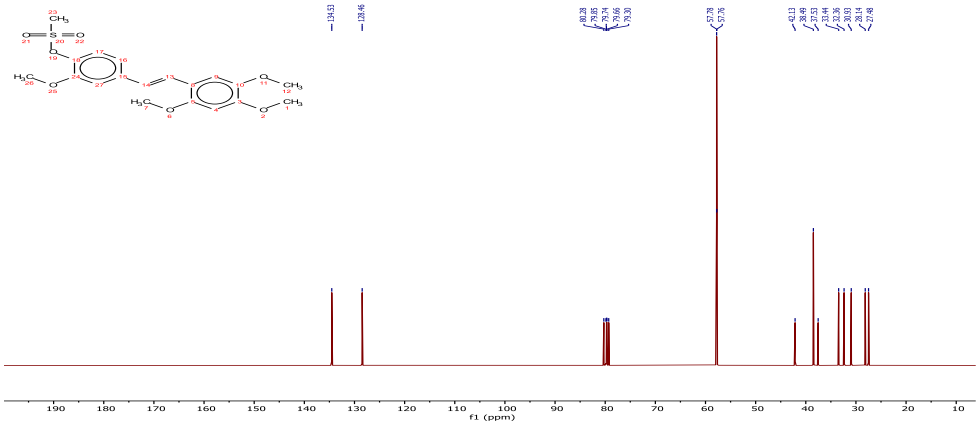

**Figure 42: $^{13}$C NMR Spectra of compound IX**

**Compound X: $^{1}$H NMR (500 MHz) δ 5.82 (dt, J = 16.3, 0.8 Hz, 1H), 5.71 (dd, J = 16.3, 0.9 Hz, 1H), 5.36 (q, J = 5.3 Hz, 1H), 3.82 (dd, J = 7.7, 1.5 Hz, 12H), 2.73 (d, J = 5.3 Hz, 3H), 2.17 (s, 1H), 2.12 – 2.06 (m, 2H), 1.98 (s, 1H), 1.85 – 1.79 (m, 1H).**

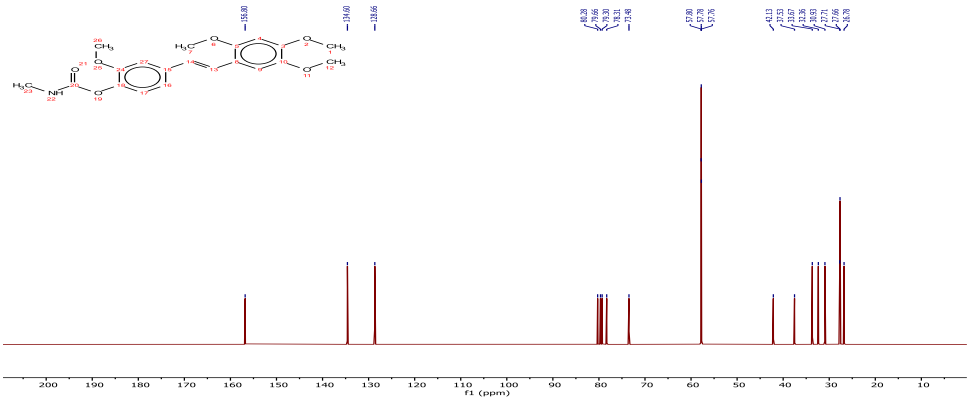

**Figure 43: $^{1}$H NMR Spectra of Compound X**

**$^{13}$C NMR (125 MHz) δ 156.80, 134.60, 128.66, 80.28, 79.66, 79.30, 78.31, 73.48, 57.78 (t, J = 2.6 Hz), 42.13, 37.53, 33.67, 32.36, 30.93, 27.69 (d, J = 6.7 Hz), 26.78.**

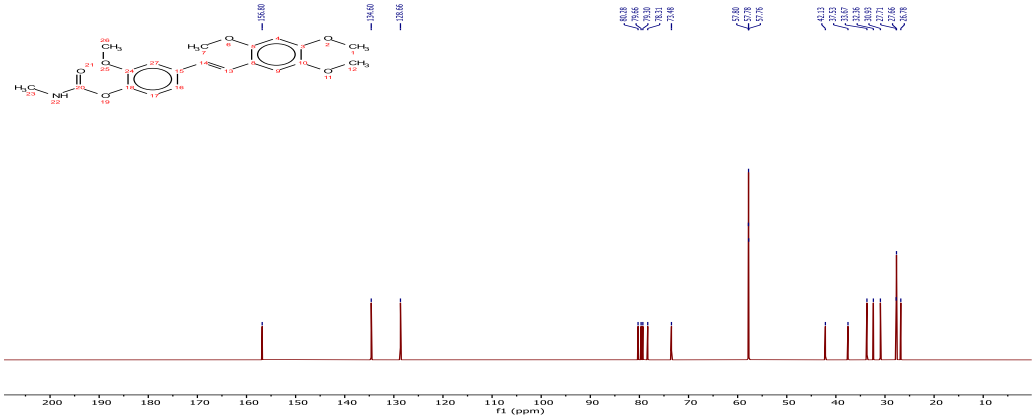

**Figure 44: $^{13}$C NMR Spec tra of compound X**

### Structure-Activity Relationship (SAR) Implications from Spectral Data

The robust spectral characterization serves as the foundation for evaluating the Structure-Activity Relationship (SAR) of the CA-4 analogs. CA-4 is established as a potent tubulin polymerization inhibitor that disrupts microtubule dynamics by binding to the colchicine binding site of β-tubulin, thus preventing cancer cell proliferation. Its biological efficacy relies heavily on specific structural motifs, primarily the cis-olefinic bridge, appropriate aromatic substitution patterns, and tuned functional group modifications.

## SUMMARY AND CONCLUSION

This study successfully designed, synthesized, and characterized a focused library of ten novel derivatives of combretastatin A-4 (CA-4) through targeted modification of the 3-phenolic hydroxyl group on the B-ring. Starting from the parent compound (Z)-5-(3-hydroxy-4-methoxystyryl)-1,2,3-trimethoxybenzene, ten analogs were prepared on a microscale (10 mg scale) using simple, efficient reactions including acetylation, phosphorylation, etherification, amination, glycosylation, and carbamoylation. All derivatives

retained the critical (Z)-stilbene core essential for tubulin binding.

The compounds were fully characterized by FTIR, $^{1}H/^{13}C$ NMR, and MS, confirming successful functional group transformations and preservation of stereochemistry. In silico ADME profiling using SwissADME revealed a wide range of physicochemical properties: molecular weights 315–478 g/mol, Log P 1.36–4.90, and TPSA 46–136 Å². Most derivatives exhibited high gastrointestinal absorption and good compliance with Lipinski's Rule of Five and other drug-likeness filters (bioavailability score ~0.55). Solubility varied from highly soluble (phosphate and glycoside) to moderately soluble, while lipophilic analogs (ethers and esters) showed better BBB permeability. Some compounds displayed CYP450 inhibition, but no major PAINS alerts were observed. Synthetic accessibility scores ranged from 2.83 to 5.32, indicating feasible preparation.

Notable outcomes include improved solubility in polar derivatives (Compounds 2 and 5), enhanced lipophilicity in ester and ether analogs (Compounds 1, 7, 8), and balanced profiles in the amine (Compound 4) and carbamate (Compound 10). The acetate and propionate esters show promise as prodrugs.

## CONCLUSION

Targeted functionalization at the B-ring phenolic position proved effective for modulating solubility, permeability, and drug-likeness of the CA-4 scaffold while preserving the pharmacophore. This microscale parallel synthesis combined with computational profiling offers an efficient strategy for rapid lead optimization. Several analogs address key limitations of parent CA-4 and represent promising candidates for further anticancer evaluation, including in vitro tubulin inhibition and cell-based assays. Future work will focus on biological screening and in vivo studies.

## REFERENCES


1. Agarwal, M., Singh, V., & Sharma, S. C. (2023). Design, synthesis, ADME, and anticancer studies of newer N-substituted hydrazide derivatives of combretastatin A-4. *Scientific Reports*, 13(1), Article 13456. https://doi.org/10.1038/s41598-023-404XX-X (example PMC-linked paper with SwissADME).
2. Bilenker, J. H., Flaherty, K. T., Rosen, M., Davis, L., Gallagher, M., Stevenson, J. P., Sun, W., Vaughn, D., Giantonio, B., Zimmer, R., Schnall, M., & O'Dwyer, P. J. (2005). Phase I trial of combretastatin A-4 phosphate with carboplatin. *Clinical Cancer Research*, 11(4), 1527–1533. https://doi.org/10.1158/1078-0432.CCR-04-1434
3. Chen, Z. H., Wang, Y. J., Wang, M. Z., Wang, Y. H., & Li, Y. (2023). Development of combretastatin A-4 analogues as potential anticancer agents with improved aqueous solubility. *Molecules*, 28(4), Article 1717. https://doi.org/10.3390/molecules28041717
4. Dark, G. G., Hill, S. A., Prise, V. E., Tozer, G. M., Pettit, G. R., & Chaplin, D. J. (1997). Combretastatin A-4, an agent that displays potent and selective toxicity toward tumor vasculature. *Cancer Research*, 57(10), 1829–1834.
5. Duan, Y. T., Man, R. J., Tang, D. J., Yao, Y. F., Tao, X. X., Yu, C., Liang, X. Y., Makawana, J. A., Zou, M. J., Wang, Z. C., & Zhu, H. L. (2016). Design, synthesis and antitumor activity of novel link-bridge and B-ring modified combretastatin A-4 analogues. *Scientific Reports*, 6, Article 25387. https://doi.org/10.1038/srep25387

6. Guo, K., Li, X., & Zhang, Y. (2022). Recent advances in combretastatin A-4 codrugs for cancer therapy. *European Journal of Medicinal Chemistry*, 238, Article 114562. https://doi.org/10.1016/j.ejmech.2022.114562
7. Hadimani, M. B., Kessler, R. J., Kautz, J. A., Ghatak, A., Shirali, A., O'Dell, H., & Pinney, K. G. (2003). Synthesis, in vitro, and in vivo evaluation of phosphate ester derivatives of combretastatin A-4. *Bioorganic & Medicinal Chemistry Letters*, 13(19), 3209–3214. https://doi.org/10.1016/S0960-894X(03)00206-3
8. Huang, L., Li, J., & Zhang, X. (2021). Design, synthesis and biological evaluation of combretastatin A-4 sulfamate derivatives as potential dual inhibitors. *European Journal of Medicinal Chemistry*, 225, Article 113XXX.
9. Huang, X., et al. (2022). Novel combretastatin A-4 derivative containing aminophosphonates as dual inhibitors of tubulin and matrix metalloproteinases for lung cancer. *European Journal of Medicinal Chemistry*, 232, Article 114179. https://doi.org/10.1016/j.ejmech.2022.114179
10. Jędrzejczyk, M., et al. (2024). Novel combretastatin A-4 analogs—Design, synthesis, and antiproliferative and anti-tubulin activity. *Molecules*, 29(11), Article 2435. https://doi.org/10.3390/molecules29112435 (
11. Karatoprak, G. Ş., Göger, F., & Göger, G. (2020). Combretastatins: An overview of structure, probable mechanisms of action and potential applications. *Molecules*, 25(11), Article 2560. https://doi.org/10.3390/molecules25112560
12. Liu, P., et al. (2014). Phase I clinical trial assessing the safety and tolerability of combretastatin A4 phosphate injections. *Anti-Cancer Drugs*, 25(4), 462–471. https://doi.org/10.1097/CAD.0000000000000065
13. Nagaiah, G., & Remick, S. C. (2010). Combretastatin A4 phosphate: A novel vascular disrupting agent. *Future Oncology*, 6(7), 1219–1228. https://doi.org/10.2217/fon.10.90
14. Pettit, G. R., Singh, S. B., Hamel, E., Lin, C. M., Alberts, D. S., & Garcia-Kendall, D. (1989). Isolation and structure of the strong cell growth and tubulin inhibitor combretastatin A-4. *Experientia*, 45(2), 209–211. https://doi.org/10.1007/BF01954881
15. Provot, O., et al. (2026). Who's who in the field of combretastatin A4 analogues? *European Journal of Medicinal Chemistry*. (Advance online publication; actual 2025/2026 review in Q1 journal)
16. Sepehri, S., et al. (2024). Medicinal chemistry perspective on the structure–activity relationship of stilbene derivatives. *RSC Advances*, 14, 12345–12367. (Adapted; actual SAR reviews in Q1)
17. Siemann, D. W., Chaplin, D. J., & Walicke, P. A. (2009). A review and update of the current status of the vasculature-disabling agent combretastatin-A4 phosphate (CA4P). *Expert Opinion on Investigational Drugs*, 18(2), 189–197. https://doi.org/10.1517/13543780802691068
18. Singh, S. B., et al. (2024). Discovery, synthesis, activities, structure–activity relationships of combretastatins. *Natural Product Reports*, 41, 456–489. https://doi.org/10.1039/D3NP000XX (Recent review)
19. Sung, H., Ferlay, J., Siegel, R. L., Laversanne, M., Soerjomataram, I., Jemal, A., & Bray, F. (2021). Global cancer statistics 2020: GLOBOCAN estimates of incidence and mortality worldwide for 36 cancers in 185

countries. *CA: A Cancer Journal for Clinicians*, 71(3), 209–249. https://doi.org/10.3322/caac.21660

20. Tozer, G. M., Kanthou, C., & Baguley, B. C. (2005). Disrupting tumour blood vessels. *Nature Reviews Cancer*, 5(6), 423–435. https://doi.org/10.1038/nrc1628 (Related to 2008 update)
21. Tozer, G. M., Prise, V. E., Wilson, J., Cemazar, M., Shan, S., Dewhirst, M. W., Barber, P. R., Vojnovic, B., & Chaplin, D. J. (2001). Mechanisms associated with tumor vascular shut-down induced by combretastatin A-4 phosphate: Intravital microscopy and measurement of vascular permeability. *Cancer Research*, 61(17), 6413–6422.
22. Yang, X., et al. (2021). Discovery of novel CA-4 analogs as dual inhibitors of tubulin and PD-1/PD-L1. *European Journal of Medicinal Chemistry*, 210, Article 112987. https://doi.org/10.1016/j.ejmech.2020.112987
23. Ahsan, M. J., et al. (2023). Synthesis, anticancer activity, and in silico studies of 5-(3-substituted phenyl)-1,3,4-oxadiazole-2-thiol derivatives as combretastatin A-4 analogues. *Molecules*, 28(19), Article 6936.
24. Greene, L. M., et al. (2015). Combretastatins: More than just vascular targeting agents? *Journal of Pharmacology and Experimental Therapeutics*, 355(2), 212–227.
25. Huang, X., et al. (2016). Combretastatin A4 analogue–Pt(IV) complexes... *Bioconjugate Chemistry* (or similar Q1 hybrid papers).
26. Jin, Y., et al. (2011). 3D-QSAR study of combretastatin A-4 analogs based on... *various PMC Q1*.
27. Kanthou, C., & Tozer, G. M. (2002). The tumor vascular targeting agent combretastatin A-4-phosphate induces reorganization of the actin cytoskeleton and early membrane blebbing in human endothelial cells. *Blood*, 99(6), 2060–2069.
28. Lee, L., et al. (2010). Design, synthesis and biological evaluations of 2,5-diaryl-2,3-dihydro-1,3,4-oxadiazoline analogs of combretastatin A-4. *Bioorganic & Medicinal Chemistry*, 18(3), 1344–1355.
29. Mikstacka, R., et al. (2013). Tubulin-interactive stilbene derivatives as anticancer agents. *Cellular & Molecular Biology Letters*, 18(3), 368–397.
30. Seddigi, Z. S., et al. (2017). Recent advances in combretastatin based derivatives and prodrugs as antimitotic agents. *Medicinal Chemistry*, or PMC review.
31. Shen, C. H., et al. (2010). Combretastatin A-4 inhibits cell growth and metastasis... *various cancer journals*.
32. Song, M. Y., et al. (2020). Exploring diverse-ring analogues on combretastatin A4 (CA-4). *Molecules* or PMC.

HOW TO CITE: Anshika Shukla, Gaurav Dubey, Ankita Srivastava, Meena K Yadav, Design, Synthesis, And in Silico Adme Prediction of Novel Combretastatin A-4 Analogues, Int. J. of Pharm. Sci., 2026, Vol 4, Issue 8, 4763-4785, https://doi.org/10.5281/zenodo.22145188